The Astrophysical Journal, 749:107 (13pp), 2012 April 20 doi:10.1088/0004-637X/749/2/107

BROADBAND JET EMISSION IN YOUNG AND POWERFUL RADIO SOURCES: THE CASE OF THE COMPACT STEEP SPECTRUM QUASAR 3C 186

Giulia Migliori[1,2], Aneta Siemiginowska[1], and Annalisa Celotti[2]
[1] Harvard-Smithsonian Center for Astrophysics, 60 Garden Street, Cambridge, MA 02138, USA; migliori@cfa.harvard.edu
[2] SISSA, Via Bonomea 265, I-34136 Trieste, Italy
Received 2011 August 27; accepted 2012 February 11; published 2012 March 28

ABSTRACT

We present the X-ray analysis of a deep (∼200 ks) *Chandra* observation of the compact steep spectrum radio-loud quasar 3C 186 ($z = 1.06$) and investigate the contribution of the unresolved radio jet to the total X-ray emission. The spectral analysis is not conclusive on the origin of the bulk of the X-ray emission. In order to examine the jet contribution to the X-ray flux, we model the quasar spectral energy distribution, adopting several scenarios for the jet emission. For the values of the main physical parameters favored by the observables, a dominant role of the jet emission in the X-ray band is ruled out when a single-zone (leptonic) scenario is adopted, even including the contribution of the external photon fields as seed photons for inverse Compton emission. We then consider a structured jet, with the blazar component that—although not directly visible in the X-ray band—provides an intense field of seed synchrotron photons Compton-scattered by electrons in a mildly relativistic knot. In this case, the whole X-ray emission can be accounted for if we assume a blazar luminosity within the range observed from flat spectrum radio quasars. The X-ray radiative efficiency of such a (structured) jet is intimately related to the presence of a complex velocity structure. The jet emission can provide a significant contribution in X-rays if it decelerates within the host galaxy on kiloparsec scales. We discuss the implications of this model in terms of jet dynamics and interaction with the ambient medium.

Key words: galaxies: jets – quasars: individual: (3C 186) – X-rays: galaxies

Online-only material: color figures

1. INTRODUCTION

Extragalactic jets have been observed on many physical scales and they often extend to distances of hundreds of kiloparsec from the nucleus (Bridle et al. 1984; Zensus 1997). Although radio jets have been known for several decades, only the *Chandra X-ray Observatory* observations have revealed their X-ray emission on large scales (see, for a review, Harris & Krawczynski 2006).

The broadband emission of bright features observed in jets can be usually—though not uniquely—well accounted for by a two-component model: a low-energy synchrotron component and a high-energy one due to Compton (IC) upscattering of seed photons off relativistic leptons. The seed photons can be produced both "locally" in the jet (synchrotron self-Compton, SSC, Maraschi et al. 1992; Bloom & Marscher 1996) and externally. At 100 kpc scales, the X-ray emission of jets in powerful Fanaroff–Riley II (FRII) sources might be explained by the inverse Compton (IC) scattering of cosmic microwave background (CMB) photons (Tavecchio et al. 2000; Celotti et al. 2001; Siemiginowska et al. 2002; Sambruna et al. 2004). At parsec (and smaller) scales, the jet radiation could be due to IC scattering of photons that originated in disk, broad emission line regions, or hot dust (see Dermer & Schlickeiser 1993; Sikora et al. 1994; Ghisellini & Madau 1996; Błażejowski et al. 2004).

However, in radio-loud (RL) quasars the parsec scale jets remain spatially unresolved at X-ray energies and often the high-energy spectral information is limited by photon statistics and broadband coverage. As a consequence, it is hard to disentangle the contribution of the non-thermal (and relativistically beamed) emission of the small-scale jet from the one related to the accretion processes (either the X-ray thermal emission of the innermost part of the disk or that resulting from Comptonization of disk photons by electrons in a hot corona).

In the nuclear region, evidence for the contribution of X-ray emission from jets comes from comparative studies of radio-quiet (RQ) and RL quasars, as RL quasars display an X-ray excess with respect to the RQ ones, which is most likely associated with the jet (Zamorani et al. 1981; Worrall et al. 1987; Miller et al. 2011, and references therein). Because the jet emission is anisotropic, its relevance depends on the orientation of the jet axis with respect to the observer's line of sight. The presence of a non-thermal component is also supported by the fact that RL quasars are X-ray brighter (with respect to their optical luminosity) for increasing values of the radio-loudness parameter, RL[3] (see Miller et al. 2011).

In young and compact radio sources, the situation is even more complex. Due to their small linear sizes ($\lesssim$20 kpc), the entire radio structure of gigahertz-peaked and compact steep spectrum[4] (GPS and CSS) radio sources is typically enclosed in a region corresponding to the unresolved X-ray core of a giant quasar/radio source (Siemiginowska 2009). Thus, studies to understand the origin of their X-ray emission (Guainazzi et al. 2006; Vink et al. 2006; Siemiginowska et al. 2008; Tengstrand et al. 2009) mainly rely on the analysis of the spectral features, which is hampered by the limited statistics; furthermore, there is (as of yet) no information on possible γ-ray emission, which would indicate the contribution of non-thermal radiation from jets. As a consequence, the origin of the bulk of the X-ray radiation in these objects is still unclear. Understanding its origin in young sources is the key to addressing several questions, such as how the source is interacting with the environment in its

[3] The radio-loudness parameter, RL, is defined as the logarithmic ratio of the monochromatic core fluxes at 5 GHz and 2500 Å (Kellermann et al. 1989).
[4] These radio sources are characterized by a linear size of $\lesssim$ 20 kpc and a power at 1.4 GHz $P_{1.4\,\mathrm{GHz}} \geqslant 10^{32}$ erg s^{-1} Hz^{-1}. They typically display convex radio spectra with turn over frequencies between ∼0.1 and ∼1 GHz (see O'Dea 1998, for a review).

initial phase of expansion and how it will evolve. Furthermore, estimating the bolometric jet emission could be a plausible indicator of the jet power and the fate of the radio source itself.

From a statistical point of view, Tengstrand et al. (2009) found that GPS *galaxies* have an intrinsic X-ray luminosity comparable to FRII radio galaxies, where the bulk of the X-rays is generally related to the disk–corona system. The location of GPS galaxies in the X-ray to [O III] luminosity ratio versus column density plane is also found to be coherent with this scenario. On the other hand, the authors point out that GPS galaxies seem to follow the same 2–10 keV and 5 GHz core luminosity correlation of Fanaroff–Riley I (FRI) radio galaxies (Chiaberge et al. 1999; Hardcastle & Worrall 2000), which points to a non-thermal, jet-related origin of the X-ray emission.

A significant level of X-ray flux can be produced via IC of different seed photons in the compact lobes of GPS radio galaxies (Stawarz et al. 2008). Given the typical GPS linear sizes ($\lesssim$1 kpc), the nuclear photon fields, e.g., optical–UV disk and IR torus photons, are intense enough to provide, when Comptonized, X-ray luminosities of the order of 10^{44}–10^{46} erg s^{-1} (Stawarz et al. 2008). The model satisfactorily accounts for the properties of a sample of GPS galaxies with compact-symmetric-object morphology (Ostorero et al. 2010) whose emission is presumably not strongly beamed. For the case of a powerful (i.e., with a jet kinetic power $L_{\rm kin} > 10^{46}$ erg s^{-1}) and nearby ($\lesssim$1 Gpc) GPS source, the model by Stawarz et al. (2008) also predicts γ-ray fluxes possibly detectable with the Large Area Telescope on board the *Fermi* satellite (see also the model results for the case of 4C +55.17; McConville et al. 2011).

In the case of GPS and CSS *quasars*, the closer jet alignment to the line of sight should favor the beamed-jet component. This is certainly observed in the radio band (Fanti et al. 1990), while the X-ray behavior remains more elusive. The median X-ray photon index, $\langle\Gamma_X\rangle = 1.84 \pm 0.24$, in the GPS and CSS quasar sample observed with *Chandra* (Siemiginowska et al. 2008) is larger than the typical index of RL quasars ($\langle\Gamma_X\rangle = 1.55 \pm 0.17$; Belsole et al. 2006). Also, the average optical-to-X-ray luminosity ratio[5] $\langle\alpha_{OX}\rangle = 1.53 \pm 0.24$ agrees with the median value found for RQ quasars ($\langle\alpha_{OX}\rangle = 1.49 \pm 0.19$; Kelly et al. 2007; Sobolewska et al. 2009) pointing to an accretion-related origin. However, in the majority of cases we still lack the detection of characteristic features associated with the accretion flow, chiefly an Fe Kα fluorescent emission line associated with a reflection component suggesting that a jet X-ray component contaminates the observed spectrum. Interestingly, the sources of the sample observed with *Chandra* appear to be more RL than their giant counterparts (Siemiginowska et al. 2008). And indeed, evolutionary models predict that the extended components of radio sources emit more efficiently during the initial phase of expansion (Begelman 1999). Furthermore, there are examples of CSS quasars whose X-ray spectrum displays a flat component in the hard X-rays, interpreted as emission from the base of the jet (e.g., 3C 48, Worrall et al. 2004).

In this context, we aim at studying the possible jet contribution in a sample of young and compact radio sources, for which we have a reasonable multi-band coverage of the spectral energy distributions (SEDs), by modeling their broadband emission. As a pilot case, we start our investigation from the case of 3C 186, a young RL quasar with a knotty radio jet that is unresolved in the *Chandra* image. Interestingly, 3C 186 is among the few quasars found in an X-ray cluster at "high" redshift ($z = 1.06$). Hence, constraining whether the bulk of the quasar X-ray emission is thermal or non-thermal can also provide information on the jet power, and in turn unveil the main channel through which the source interacts with the galactic and cluster environment.

We model the jet SED as synchrotron and IC emission, taking into account the main local and external radiation fields which can act as seed photons. As the assumption that a single (homogeneous) emitting region dominates the jet SED in quasars is still a matter of debate (Ghisellini et al. 2009; Sikora et al. 2009; Poutanen & Stern 2010; Marscher et al. 2010; Lyutikov & Lister 2010, and references therein), we also treat the case of a jet with a complex velocity structure. We consider the presence of two emitting regions moving with different velocities and take into account the relative effects on the emission via IC. We also examine the implications of such a scenario in terms of source dynamics and energetics.

The paper is organized as follows. After reviewing the 3C 186 properties (Section 2), in Section 3 we focus on the *Chandra* observations and the corresponding X-ray spectral analysis. The model for the broadband emission from the quasar jet is described in Section 4. The results of the SED modeling and the consequences in terms of jet power are discussed in Section 5. We finally summarize our findings in Section 6. Throughout this work, we assume the following cosmological parameters: $H_0 = 71$ km s^{-1} Mpc^{-1}, $\Omega_M = 0.27$, and $\Omega_\Lambda = 0.73$.

2. THE RADIO-LOUD QUASAR 3C 186

3C 186 is a luminous quasar ($L_{\rm bol} \sim 10^{47}$ erg s^{-1}; Siemiginowska et al. 2005) with a compact FRII morphology, located at redshift $z = 1.067$. The radio structure is characterized by two components, identified as the radio lobes, separated by $\sim$2″, and a knotty jet connecting the core to the northwest lobe (Spencer et al. 1991).

The steep radio spectrum, the relatively small projected linear size ($\sim$16 kpc), and an estimated spectral age of $\sim 10^5$ yr (Murgia et al. 1999) indicate that the source belongs to the class of CSS radio quasars.

At optical–UV wavelengths, 3C 186 has a typical quasar spectrum, dominated by a luminous big blue bump component ($L_{\rm UV} = 5.7 \times 10^{46}$ erg s^{-1}; Siemiginowska et al. 2005) and broad optical emission lines (Netzer et al. 1996; Simpson & Rawlings 2000; Kuraszkiewicz et al. 2002; Evans & Koratkar 2004).

In the X-ray band, the quasar has been observed twice with the *Chandra* satellite. The first *Chandra* observation led to the discovery of diffuse ($r \gtrsim 500$ kpc) X-ray emission surrounding the quasar, interpreted as thermal radiation from the intracluster medium (Siemiginowska et al. 2005). This is one of the few cases of a quasar in a luminous X-ray cluster environment at $z > 1$. The quasar is bright in X-rays (L_X(2–10 keV) $= 1.2 \times 10^{45}$ erg s^{-1}) and dominates over the thermal cluster emission in the central region (the X-ray diffuse emission is $\lesssim$3% of the total X-ray flux; Siemiginowska et al. 2010). A detailed study of the second deep *Chandra* observation—dealing with the extended component—shows that the cluster gas temperature drops from $kT \sim 8$ keV in the outer parts of the cluster to $kT \sim 3$ keV in the central region, indicating a strong cooling core (Siemiginowska et al. 2010). The authors argued that the cooling gas could provide enough fuel to support the growth of the central supermassive black

[5] The optical-to-X-ray luminosity ratio, α_{OX} (Avni & Tananbaum 1982), is defined as $\log[F(2500\,\text{Å})/F(2\,\text{keV})]/2.605$ in rest frame, where $F(2500$ Å) and $F(2$ keV) are monochromatic fluxes in cgs units at 2500 Å and 2 keV, respectively.

Table 1
Chandra Observations of 3C 186

Obs. Date	ObsID	Livetime (s)	Source Counts[a] (Total)	Source Counts[b] (Background Subtracted)
2007 Dec 3	9407	66269	3630	3595 ± 66
2007 Dec 6	9774	75141	4037	3996 ± 70
2007 Dec 8	9775	15934	825	816 ± 32
2007 Dec 11	9408	39623	2054	2054 ± 50
2002 May 16[c]	3098	34436	1719	1699 ± 46

Notes.
[a] Total (source and background) counts within the energy range 0.5–7.0 keV in the selected circular region centered on the quasar ($r = 1\farcs5$).
[b] Background-subtracted counts in the selected circular region centered on the quasar ($r = 1\farcs5$).
[c] The 2002 *Chandra* observation was reprocessed applying the newest calibration. The same radius as for 2007 *Chandra* observations was assumed for the extraction region.

hole. The quasar, in turn, would provide the energy/momentum critical to the possible radiative feedback which is still not well understood.

The morphological study of the X-ray emission of the quasar is hampered by the small angular dimensions of the radio source. The X-ray spectral analysis based on the first *Chandra* observation data set was not conclusive on the nature and origin of the X-ray emission. The best-fit model, a simple power law with a steep spectral index ($\Gamma_X = 2.01 \pm 0.07$; Siemiginowska et al. 2005), is compatible with being both non-thermal emission from the extended radio components, namely jet and lobes, as well as a nuclear emission related to the disk photons Comptonized by electrons in a hot corona. The presence of the Fe Kα line in the quasar X-ray spectrum, which would point to the nuclear origin hypothesis, was uncertain due to the limited statistics. We start our study with a description and analysis of the second *Chandra* observation of the quasar emission. We also use the archival data from the first observation which we reprocessed in order to apply the updated calibration.

3. *CHANDRA* OBSERVATIONS

3.1. Observations and Data Analysis

3C 186 was observed for the second time with the *Chandra* Advanced CCD Imaging Spectrometer (Weisskopf et al. 2002) on 2007 December 3. The ∼198 ks long observation was segmented into four intervals (see Table 1) due to *Chandra* observing constraints (Proposer's Observatory Guide).

The source was located on the ACIS-S backside-illuminated chip S3 and was offset by ∼1′ in *Y*-coordinates from the default aim-point position to make sure that the cluster is not affected by a chip gap. The observation was made in full-window mode and VFAINT mode, which ensures a more efficient way of determining the background events and cleaning background, especially at higher energies.

We performed the X-ray data analysis using CIAO version 4.3 and the calibration files from the last CALDB release (4.4.2). This version includes the upgrade of the ACIS-S contamination file (*acisD1999-08-13contamN0006.fits*), which accounts for the temporal degradation of the detector quantum efficiency due to materials deposition on the ACIS chips or optical blocking filters.

We ran the `chandra_repro` script available in CIAO 4.3 to reprocess the data and apply the newest calibration. We used the default options "check_vf=yes" and "pix_adj=EDSER" to obtain the highest resolution image data. We also investigated the light curve and found no periods of significant background flares or quasar variations. We also reprocessed the archival data from the first *Chandra* observation performed on 2002 May 16 and applied the newest calibration. The 2002 observation was affected by a background flare and we used the standard filtering of the data based on the background light curve. The filtered quasar spectrum has a background rate of <0.0007 counts s^{-1} in the quasar region and the effective exposure time of 34.4 ks.

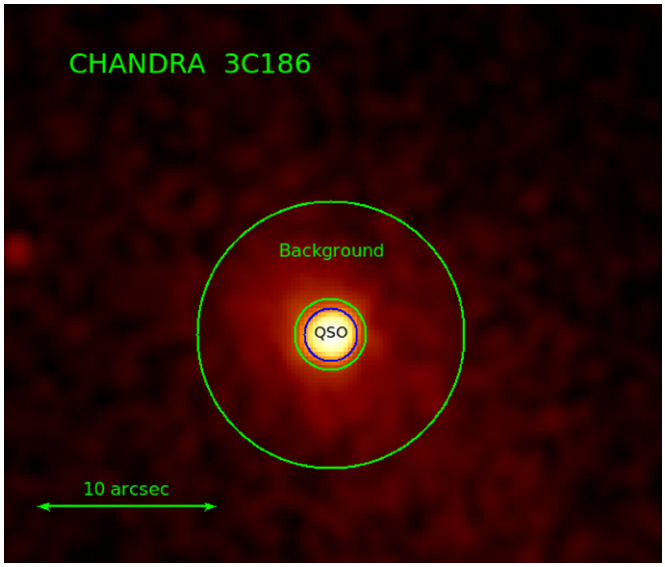

Figure 1. Smoothed exposure-corrected image of the *Chandra* ACIS-S observation of 3C 186 in the 0.5–7 keV energy range. The regions selected for the quasar and background spectra are marked by a blue circle and a green annulus, respectively.
(A color version of this figure is available in the online journal.)

Figure 1 shows the *Chandra* ACIS-S image (2007 epoch) in the 0.5–7.0 keV band: both the central quasar and the extended cluster emission are clearly visible. The whole quasar structure is included in a circular region of radius smaller than 2″. The diffuse cluster emission extends to ∼500 kpc from the central quasar. Hereafter, we present the analysis on the quasar, always indicated as 3C 186, while we refer to Siemiginowska et al. (2010) for the analysis of the X-ray data of the cluster.

3.2. X-Ray Spectral Analysis

The 3C 186 radio source has a total angular size of ∼2″. Its complex radio structure is not resolved out in the X-ray due to the *Chandra* angular resolution (∼1″). We defined the quasar emission region as a circle, centered on the source coordinates, with a radius of $r = 1\farcs5$, in order to collect 98% of the whole source emission. An annulus surrounding the quasar with inner and outer radii set at 2″ and $7\farcs5$ was selected for the background. In this way, a source spectrum and the relative background data set were obtained for each of the five (1+4) observations. The total counts for each data set are shown in Table 1. Because of the increase of the background at low and high energies, we restricted the analysis to the 0.5–7.0 keV energy band.

We used Sherpa 4.3 (Freeman et al. 2001) to model simultaneously the four source spectra obtained in the individual observations during the 2007 epoch. We used Cash statistics and the Nelder–Mead Simplex optimization method (Nelder & Mead 1965) to fit the models to the spectral data. We also applied the

Table 2
Best-fit Power-law Model[a]

ObsID	Γ_X	Norm (10^{-5} photons cm^{-2} s^{-1})	cstat (442 dof)[b]
9407	1.94 ± 0.04	8.69 ± 0.27	483.1
9774	1.90 ± 0.04	8.39 ± 0.28	496.3
9775	1.80 ± 0.10	7.83 ± 0.54	479.4
9408	1.94 ± 0.06	8.21 ± 0.32	479.4
All[c]	1.92 ± 0.03	8.42 ± 0.16	3274.46 (3548)
Background Model			
ObsID	kT (keV)	Norm (10^{-4} photons cm^{-2} s^{-1})	cstat (442 dof)
9407	$5.90^{+0.98}_{-0.84}$	$1.89^{+0.14}_{-0.12}$	395.7
9408	$5.8^{+1.3}_{-1.0}$	$2.02^{+0.19}_{-0.16}$	364.8
9774	$4.78^{+0.61}_{-0.52}$	$2.11^{+0.14}_{-0.13}$	326.7
9775	$5.89^{+2.9}_{-1.4}$	$1.88^{+0.27}_{-0.26}$	266.0
All[d]	$5.27^{+0.7}_{-0.4}$	$2.01^{+0.08}_{-0.09}$	1358.9 (1774)
Power-law Model Parameters for the fixed Background Model[e]			
ObsID	Γ_X	Norm (10^{-5} photons cm^{-2} s^{-1})	cstat (442 dof)
3098	2.03 ± 0.07	$7.33^{+0.32}_{-0.31}$	468.9
9407	$1.94^{+0.05}_{-0.06}$	$8.67^{+0.33}_{-0.30}$	483.0
9774	$1.90^{+0.06}_{-0.05}$	$8.36^{+0.35}_{-0.24}$	496.3
9775	$1.82^{+0.10}_{-0.13}$	$7.97^{+0.46}_{-0.77}$	447.8
9408	$1.93^{+0.09}_{-0.06}$	$8.07^{+0.56}_{-0.24}$	479.9

Notes.
[a] The equivalent hydrogen column fixed at the Galactic value of 5.64×10^{20} cm^{-2}. Uncertainties are 90% for one significant parameter. The background model was first fitted to all spectra and then fixed at the best-fit parameter values when fitting individual observations.
[b] Degrees of freedom for single spectrum fit.
[c] Excluding ObsID 3098.
[d] Best-fit parameter values of the background model of the simultaneous fit of the 2007 *Chandra* observations.
[e] The background model parameters were fixed at the values of the simultaneous best fit.

parametric model to the background data and used it in fitting the quasar spectra. All the statistical errors were calculated at 90% confidence limits for a single parameter with the `conf` routine in Sherpa.

Because the thermal cluster emission dominates the background in the vicinity of the quasar, we selected an absorbed thermal plasma model as a background model. We fitted this model to the background data first and then applied it with the appropriate scaling when fitting the quasar spectra. We recall that the cluster contribution to the quasar spectrum is negligible (Siemiginowska et al. 2010).

We assumed an absorbed power-law (*xsphabs* and *xspowerlaw* models in Sherpa) model for the quasar emission. The equivalent column was fixed at the Galactic value $N_{\rm H} = 5.64 \times 10^{20}$ cm^{-2}, calculated using COLDEN.[6] First we fitted the spectrum from each observation, then, as no significant systematic difference was found, we fitted the same power-law model to all four spectra simultaneously. The best-fit power-law model parameters are listed in Table 2. In the 0.5–7 keV energy range, $\Gamma_X = 1.92 \pm 0.03$, while the photon index of the individual observations ranges between 1.80 ± 0.08 and 1.94 ± 0.03 with the lower value for the data set having the worst signal-to-noise spectrum. An inspection below 0.5 keV of the spectrum extracted from the 9774 observation made us exclude that the residuals we see in its 0.5–0.7 energy band are related to an additional emission component. The unabsorbed fluxes between 0.5–2 keV and 2–10 keV, extrapolated from the best-fit model, are respectively $F_{0.5-2\,\rm keV} = (1.65 \pm 0.04) \times 10^{-13}$ erg cm^{-2} s^{-1} and $F_{2-10\,\rm keV} = (2.5 \pm 0.1) \times 10^{-13}$ erg cm^{-2} s^{-1}.

While the photon index is in a relatively good agreement with the results presented in Siemiginowska et al. (2005, 2008) ($\Gamma_X = 2.01 \pm 0.07$), we note some level of discrepancy between the flux values ($F_{2-10\,\rm keV} = 1.7 \times 10^{-13}$ erg cm^{-2} s^{-1}). We therefore used the reprocessed archival data from 2002 to extract the quasar spectrum in exactly the same way as in the case of the new 2007 observation. We assumed an absorbed power-law model, with the equivalent column fixed to the Galactic value, and the same background model in fitting this quasar spectrum. Our best-fit parameter values for the 2002 observation are consistent with the reported earlier results, i.e., $\Gamma_X = 2.03 \pm 0.07$ and $F_{2-10\,\rm keV} = 1.8 \pm 0.1 \times 10^{-13}$ erg cm^{-2} s^{-1} (and $F_{0.5-2\,\rm keV} = 1.36 \pm 0.05 \times 10^{-13}$ erg cm^{-2} s^{-1}). We conclude that the quasar's flux has increased by about 40% and the spectrum became slightly harder. We note that the 0.5–7 keV source count rates in the 2002 and 2007 observations are not so discrepant (0.049 ± 0.001 counts s^{-1} in the 2002 observation and between 0.051 ± 0.002 and 0.054 ± 0.001 counts s^{-1} in the 2007 ones), and the difference in the 2–10 keV flux is determined by the time-dependent calibration of ACIS-S and the flatter power-law index in the second epoch.

We checked and did not detect any significant absorbing column intrinsic to the quasar, with a 3σ upper limit to the equivalent column of hydrogen of $< 2 \times 10^{20}$ cm^{-2}. We also investigated whether there are emission features in the spectra and determined that there is no evidence for the presence of an emission line in the spectra, the detection of which, at $\sim$3 keV, was only tentative in the first *Chandra* observation (Siemiginowska et al. 2005).

In Figure 2, we show the spectra from each observation overplotted with the best-fit power-law model and the residuals. The residuals are consistent with no emission line.

4. 3C 186: MODELING X-RAY EMISSION AND BROADBAND SED

Let us consider the indicators of non-thermal X-ray emission (see Section 1) for the specific case of 3C 186. 3C 186 is a powerful radio quasar with a high radio-loudness value, RL = 3.7 (Miller et al. 2011). The source is also X-ray bright and, given the value of RL, the jet component might dominate or be important in the X-rays. On the other hand, Siemiginowska et al. (2008) have shown that its X-ray-to-optical luminosity ratio appears to be smaller with respect to the typical RL quasars (see Figure 9 in Siemiginowska et al. 2008). The steep X-ray photon index ($\Gamma = 1.92 \pm 0.03$), together with the value of the optical-to-X-ray luminosity parameter ($\alpha_{OX} = 1.74$), is more in agreement with the average values found for RQ quasars, i.e., $\Gamma_X = 2.03 \pm 0.31$ and $\alpha_{OX} = 1.49 \pm 0.19$, respectively (Kelly et al. 2007; Sobolewska et al. 2009). Note however that, albeit the limited statistics, the available X-ray spectral analysis did not reveal the typical features of accretion-related X-ray emission, most notably the Fe Kα line.

Thus, while the radio features seem to suggest a relevant jet-related X-ray emission, the optical-to-X-ray data rather support a disk–corona scenario.

[6] http://cxc.harvard.edu/toolkit/colden.jsp

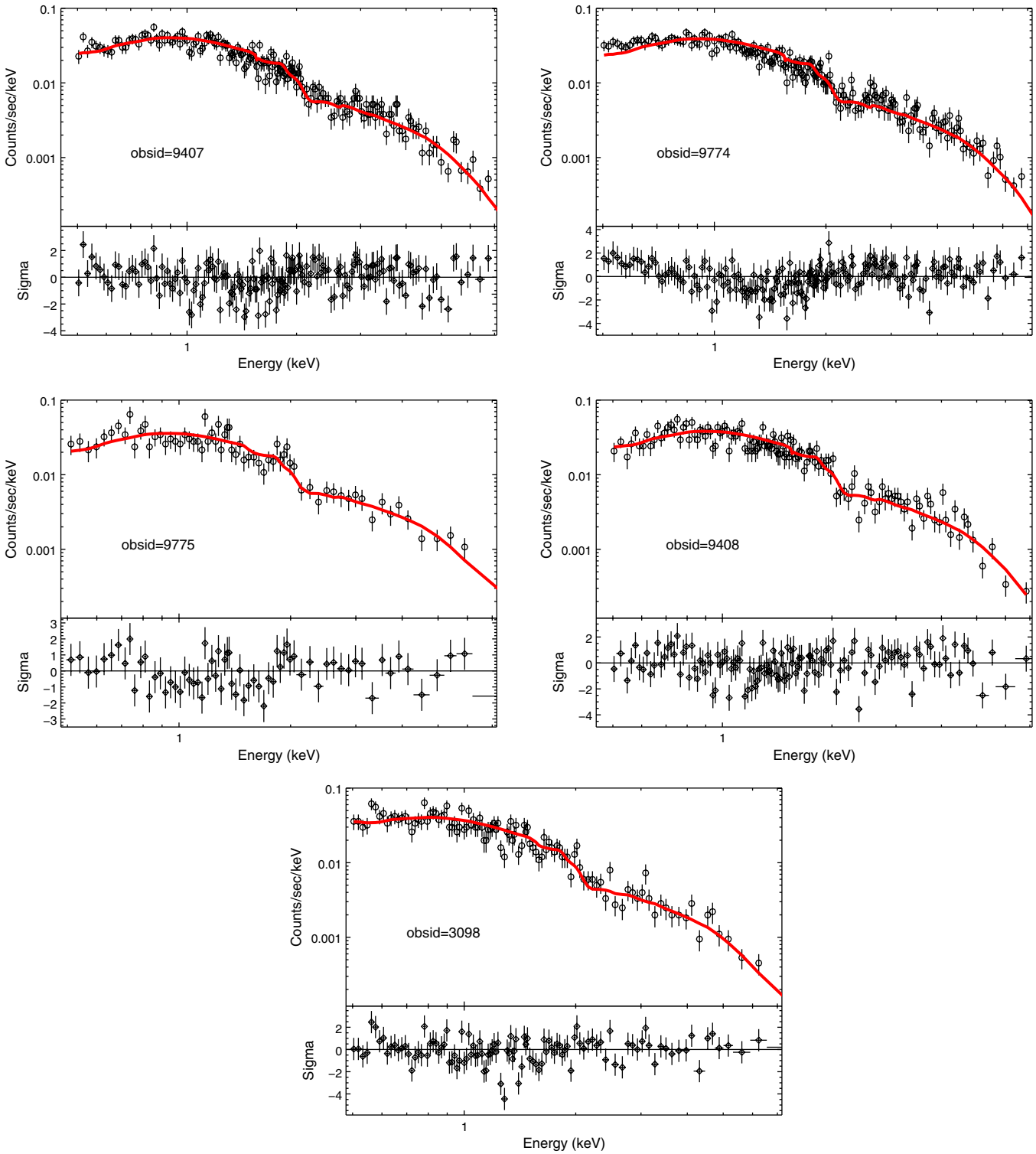

Figure 2. ACIS-S spectra in the 0.5–7.0 keV band of the five *Chandra* observations of the quasar 3C 186 with the best-fit absorbed power-law model superposed (solid line). The data were grouped to ensure a minimum signal-to-noise ratio of three per a bin. The lower panels show the residual difference between the model and the data in units of sigma. The inspection of the 9774 spectrum below 0.5 keV excludes additional source component at soft energies.

(A color version of this figure is available in the online journal.)

While both scenarios, accretion- and jet-related emission, do not exclude X-ray variability at the observed level, flux and spectral variability can be very useful to disentangle the different components in those sources where the two contributions are competing in the X-rays (as for the case of 3C 273 and in broad-line radio galaxies; see Grandi & Palumbo 2004, 2007; Kataoka et al. 2007; Sambruna et al. 2009; Chatterjee et al. 2011).

In 3C 186, the flux increases and there is a slight (although not statistically significant) indication of spectral hardening. A possibility is that the jet component is varying with respect to a steady accretion-flow continuum. Simultaneous X-ray and

high-resolution radio observations would be needed to better investigate this hypothesis and we will discuss the radio-X-ray connection in Section 5.

The core dominance[7] (CD) of the radio source is another indicator of the jet orientation, and thus of the importance of the beamed component. Fan & Zhang (2003) reported for 3C 186 a CD value of −1.66, lower than the average value found in their quasar sample, $\langle \mathrm{CD} \rangle = -0.53 \pm 0.92$. Given this CD, the quasar should be classified as a lobe-dominated source,[8] with a likely minor contribution of the beamed-jet emission to the total X-ray flux. However, the CD parameter estimate suffers from uncertainties related to, for instance, the resolution of the radio map. In addition to this, the CD parameter may not be a suitable indicator of the jet axis orientation in young radio sources. In fact, theoretical models predict that during the first stages of the radio source evolution, the extended structures, e.g., the lobes, are overpressured, and thus radio overluminous with respect to the lobes of giant radio sources (Begelman 1999).

4.1. Jet SED Modeling

The modeling of the jet broadband SED can be effective in discerning the X-ray emission components and possible jet contribution in RL quasars. This also provides us with an estimate of the jet kinetic power (and the relative contributions of particles, magnetic field, and radiation), a key quantity to investigate the dominant mode through which the radio source interacts with the surrounding medium.

We adopted a leptonic synchrotron and IC model to account for the broadband emission of the 3C 186 jet. The multi-wavelength data set allows us to constrain the most intense photon fields at different jet scales, and the available radio maps provide us with indications on the sites where the bulk of the radiative dissipation is likely to occur along the jet. The source is still embedded within the host-galaxy environment, therefore the jet is moving in a dense field of nuclear photons, namely the optical–UV disk photons, the IR-torus photons, and possibly the IR–optical starlight photons. These components, pervading the region where the jet energy dissipation occurs, are relevant for the jet IC emission and need to be evaluated.

In addition to this, we also investigated the possibility that the jet has a complex structure, with emitting regions moving at different velocities.

A structured jet has been invoked in order to efficiently produce high-energy (X- to γ-ray) emission (see Celotti et al. 2001; Stawarz & Ostrowski 2002; Georganopoulos & Kazanas 2003; Ghisellini et al. 2005) as it has been shown that jets with a velocity structure can be radiatively very efficient when a feedback is established among the regions moving at different velocities. A stratified jet, with a fast spine and a slower sheath, has been considered to solve difficulties in models that unify BL Lac objects and low-power radio galaxies (Chiaberge et al. 2000). Radio (Swain et al. 1998; Giovannini et al. 1999; Giroletti et al. 2004) and X-ray (see the case of Cen A, 3C 273, and PKS 1127−145; Worrall et al. 2008; Jester et al. 2006; Siemiginowska et al. 2007, respectively) observations support the idea of a complex jet structure, although the geometry is not still uniquely defined. On the basis of the results

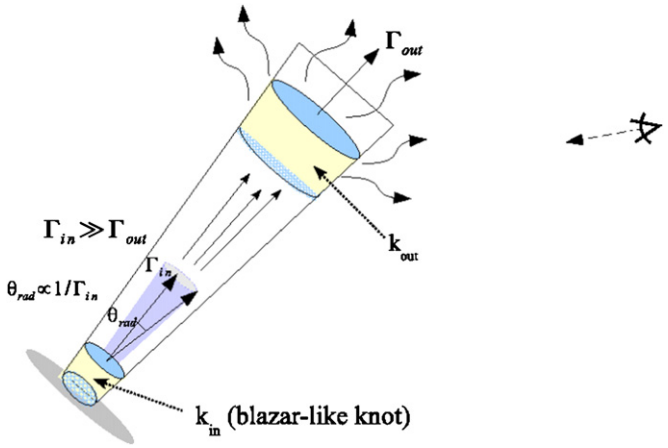

Figure 3. Sketch of the jet structure for the case of an axial velocity gradient (see Celotti et al. 2001; Georganopoulos & Kazanas 2003). We consider two regions of energy dissipation, a highly relativistic knot ($k_{\rm in}$, blazar-like region) located at the base of the jet and a second, mildly relativistic one ($k_{\rm out}$) farther out. The synchrotron radiation from the blazar-like region is mostly emitted in a narrow cone ($\theta_{\rm rad} \propto 1/\Gamma_{\rm in}$, with $\Gamma_{\rm in}$ bulk motion of the knot itself) and illuminates the second knot $k_{\rm out}$. The jet inclination with respect to the observer line of sight hides the bulk of the blazar-like emission to the observer view while the radiation from the slow-moving knot $k_{\rm out}$ is emitted quasi-isotropically.

(A color version of this figure is available in the online journal.)

of statistical studies, a velocity gradient also seems to be required in the jets of powerful radio sources: in FRII the bulk flow speed of the jet significantly changes from parsec to kiloparsec scales (Mullin & Hardcastle 2009) and in RL quasars Miller et al. (2011) infer different beaming factors for the radio and X-ray jet emission.

Models for a structured jet typically consider a velocity gradient which develops along either the jet axis (Celotti et al. 2001; Georganopoulos & Kazanas 2003) or the cross-section radius (Stawarz & Ostrowski 2002; Ghisellini et al. 2005).

Following Celotti et al. (2001), we hypothesized a jet with two emitting regions which are radiatively interacting: (1) a fast blazar-like region close to the base of the jet and (2) a slower radiating knot located farther out along the jet axis.

A sketch of the model is shown in Figure 3. The blazar-like knot, $K_{\rm in}$, is moving with a bulk Lorentz factor[9] $\Gamma_{\rm in}$ and emits via the synchrotron mechanism. The synchrotron radiation from such a region is relativistically beamed within an aperture angle $\theta_{\rm rad} \propto 1/\Gamma_{\rm in}$ and illuminates the slower, outer knot ($k_{\rm out}$). For $\Gamma_{\rm in} \gg 1$, this results in an intense external field of seed synchrotron photons in the $k_{\rm out}$ frame. The bulk of the synchrotron—and IC—emission of the blazar-like component is, however, not visible by an observer whose line of sight is not closely aligned with the jet axis (at an angle $\theta > \theta_{\rm rad}$). Conversely, he/she could detect the synchrotron and IC radiation from the slow-moving knot $k_{\rm out}$, which is emitted more isotropically. We considered this scenario for the case of 3C 186 and discuss the conditions under which a structured jet can effectively reproduce the observed X-ray emission.

4.1.1. Physical Parameters

In modeling the jet broadband SED, there are some delicate points related to necessary assumptions on the main parameters' values (the magnetic field B and electron energy distribution, EED), the geometry of the emitting region, and the spatial

[7] The core dominance parameter is defined as $\mathrm{CD} = \log(F_c/(F_{\rm tot} - F_c))$, where $F_{c/\rm tot}$ are the core and total 5 GHz flux densities in the source rest frame (Scheuer & Readhead 1979).

[8] There are several definitions of core/lobe-dominated sources. Here, we define a radio source core/lobe-dominated when its core monochromatic luminosity at 5 GHz is greater/less than half of the total radio luminosity.

[9] The bulk Lorentz factor is defined as $\Gamma = (\sqrt{1-(v/c)^2})^{-1}$ where v is the bulk velocity of the emitting plasma.

Table 3
Radio Data for 3C 186 Components

Regions	F_{600}[a] (mJy)	$\theta_1 \times \theta_2$[a] (mas^2)	$F_{1.6}$[b] (mJy)	$\theta_1 \times \theta_2$[b] (mas^2)	α_{600}^{15}	F_5[c] (mJy)	F_{15}[c] (mJy)
A(hotspot+	525	52×15	520	350×250	$\geqslant 1.2$	...	...
South lobe)	584	203×42	...	...	...	90	20(southeast)
k_1(nucleus)	abs.	...	12	...	~ 0.0	15	21
k_2(first knot)	...	...	40	93×65	$\geqslant 1.2$	...	...
k_3(second knot)	...	...	80	85×48	$\geqslant 1.2$	...	...
N-jet(k_3 to B)	...	...	130	725×100	$\geqslant 1.2$	...	...
Jet(total)	385	140×44	...	...	...	93	25(central)
B(North lobe)	315	224×83	290	460×320	$\geqslant 1.2$	...	9(northwest)

Notes.
[a] 600 MHz fluxes and angular dimensions from Nan et al. (1991).
[b] 1.6 GHz fluxes and angular dimensions from Spencer et al. (1991).
[c] 5 GHz fluxes from Ludke et al. (1998).
[d] 15 GHz fluxes (C.C. Cheung 2012, private communication).

dependence of the local and external photon densities. The angle between the jet axis and the observer's line of sight θ, and the bulk Lorentz factor Γ are fundamental but also partly degenerate parameters with respect to the observables. Multiband data and radio maps allow us to place some constraints on these quantities.

Jet radio morphology. Radio observations provide us with spatial details of the 3C 186 jet structure, necessary to constrain the physical parameters of the emitting regions. The radio map at 1662 MHz in Spencer et al. (1991) (see Figure 2 in their paper and available on NED[10]) shows a jet with two knots ($k2$ and $k3$) connected to the northern lobe B by a radio low-luminous bridge.In the southern lobe, A, observations at 600 MHz reveal the presence of a hotspot (Nan et al. 1991). The core, $k1$, is self-absorbed below 1.6 GHz. The 600 MHz, 1.6, 5, 15 GHz measurements are summarized in Table 3.

The radio surface brightness of the knots (6.62×10^{-3} mJy mas^{-2} for $k2$ and 1.96×10^{-2} mJy mas^{-2} for $k3$ at 1.6 GHz) and the hotspot (0.67 mJy mas^{-2} at 600 MHz) is higher than that of the diffuse structure (1.79×10^{-3} mJy mas^{-2}), supporting the idea that the compact substructures are the main sites of power dissipation. Therefore, in modeling the jet emission we considered only the two knots and the hotspot, and neglected the region of low radio brightness.

Jet axis inclination and bulk motion. Symmetry arguments seem to rule out a very close alignment ($\theta \leqslant 10^\circ$) of the source with the line of sight: the two lobes, A and B, are located at similar distances from the central region (respectively at 970 and 1250 mas; Spencer et al. 1991). On the other hand, the detection of broad optical lines points to a dust free view of the inner nuclear region. Thus, unless the putative "torus" has a large opening angle, the source does not lie close to the plane of sky ($\theta \lesssim 60^\circ$). The visible jet is pointing toward the lobe more distant from the core but is not on the same side of the bright hotspot. Estimates based on the one-sided Very Large Array jet give a $\theta \lesssim 30^\circ$ angle and a corresponding de-projected size of at least $\approx$30 kpc (Siemiginowska et al. 2010). The value of the CD parameter (CD $= -1.66$), albeit with uncertainties and caveats, indicates a moderate alignment along the line of sight. Thus, we assumed an inclination angle of 30° and discuss the variation of the modeling results for smaller θ.

Knot/hotspot physical parameters. We derived the de-projected distances from the radio core location of the two knots and the hotspot from the 18 cm radio data (see Table 3 in Spencer et al. 1991). For the assumed $\theta = 30^\circ$, these are $z_d(k2) \sim 2.4$ kpc, $z_d(k3) \sim 9.8$ kpc, and $z_d(hs) \sim 15.4$ kpc for $k2$, $k3$, and the hotspot, respectively. From these we calculated the physical volumes using the 1.6 GHz maps for the two knots and the 600 MHz map for the hotspot by assuming a cylindrical geometry (in Table 3 the smallest angular size corresponds to the base diameter and the longest to the height).

There is no information on the apparent motion of the jet features. The linear size to source age ratio provides us with some indications on the advanced velocity, $v_{\rm ad}$, under the relevant assumption of continuous and uniform source expansion. For a linear size between the observed 15 kpc and the de-projected (for $\theta = 30^\circ$) 30 kpc, and an estimated source age of $\sim 10^5$ yr (Murgia et al. 1999), $v_{\rm ad}$ ranges between $0.24c$ and $0.49c$. We note that hotspots' advance velocities of GPS sources are about 0.1–0.2c (Owsianik et al. 1998; Gugliucci et al. 2005), while radio and statistical studies suggest mildly relativistic speeds ($\approx 0.5c$ to $\approx 0.8c$) of the jet at kiloparsec scales (Wardle & Aaron 1997; Hardcastle et al. 1999; Mullin & Hardcastle 2009; Miller et al. 2011). Following Mullin & Hardcastle (2009), we assumed a bulk Lorentz factor of 1.4 for the knots and adopted an upper limit of $v_{\rm ad} = 0.1c$ for the hotspot Lorentz velocity.

Magnetic field and EED. The magnetic field, B, and particle energy densities, U_e, were initially calculated under an equipartition assumption and normalized to the radio-observed fluxes. As there is no evidence of a complex spectral shape from the observed SED, we assumed a simple power law for the EED, $N(\gamma) = K\gamma^{-p}$: p is derived from the lower limit of the radio spectral index (i.e., $\alpha_r \leqslant 1.2$) $p = 2\alpha_r + 1 = 3.4$, and the minimum and maximum Lorentz factors were set equal to $\gamma_{\rm min} \sim 75$ and $\gamma_{\rm max} \sim 10^5$. The adopted α_r is steeper than the X-ray spectral index ($\alpha_X = \Gamma_X - 1 = 0.92 \pm 0.03$). Nevertheless, the two spectral indexes are not necessarily expected to be the same if the X-ray flux is contributed by different competing components (e.g., the X-ray accretion continuum) and/or the X-ray emission is produced by the "tails" of the particle and seed photon distributions (as indeed is the case here, see Figure 5).

4.1.2. Photon Fields

In this section, we evaluate the energy densities of the local and external photon fields which can act as target photons for the IC mechanism (see Celotti et al. 2001). As mentioned, we assumed that the bulk of the jet dissipation is spatially localized at the position of the radio compact features, namely

[10] http://ned.ipac.caltech.edu/img11/1991MNRAS.250..225S/3C_186c:I:18cm:1991ssf.jpg

the two knots and the hotspot. In the following, we inferred the energy densities of each photon field in the knot/hotspot reference frame (primed quantities), while the luminosities are the intrinsic ones in the reference frame of the source of photons ($L^i_{\rm source}$).

Local fields. The energy density of the synchrotron photons produced locally in each knot and the hotspot, $U'_{\rm SSC}$, was calculated for a cylindrical geometry:

$$U'_{\rm SSC} \sim \frac{3L^i_{\rm syn}}{4\pi Rhc}, \quad (1)$$

where R is the cross-section radius and h is the height of the cylinder (see Table 3), and $L^i_{\rm syn}$ is the integrated synchrotron luminosity of the knots/hotspot estimated from the assumed EED and magnetic field ($L^i_{\rm syn}(k2/k3/{\rm hotspot}) = 3.5\times10^{43}/9\times 10^{43}/1.6\times10^{44}$ erg s^{-1}).

Nuclear fields, starlight, and CMB. The photon energy densities produced in the disk and torus as seen in the knot/hotspot frame ($U'_{\rm disk}$ and $U'_{\rm torus}$ for the disk and the torus, respectively) depend on the distance z_d of the knot/hotspot from the disk/torus and on the bulk motion of the knot/hotspot ($\Gamma_{\rm (knot/hotspot)}$). At the estimated distances of the jet knot/hotspot, the disk and the torus can be treated as point-like sources, and thus

$$U'_{\rm disk/torus} \sim \frac{L^i_{\rm disk/torus}}{4\pi z_d^2 c\Gamma^2_{\rm (knot/hotspot)}}, \quad (2)$$

where $L^i_{\rm disk/torus}$ is the intrinsic luminosity of the disk/torus.

The estimated disk luminosity of 3C 186 is $L^i_{\rm disk} = 5.7\times10^{46}$ erg s^{-1} (Siemiginowska et al. 2005).

The bulk of the IR luminosity of 3C 186 is likely to be thermal, originating as disk radiation reprocessed in the dusty torus. Comparative studies of quasars and radio galaxies at redshift $z > 1$ show that in quasars the heated-dust emission is typically a factor of 5–10 above the galaxy contribution (Haas et al. 2008). In order to account for the torus' vertical dimension, we assumed that all the dust emission comes from a height smaller than 10 pc over the disk position.

The K-band magnitude of the 3C 186 host galaxy, $m_K({\rm gal}) = 17.1$ (Carballo et al. 1998), can be considered as a good indicator of the starlight emission. The galaxy contribution corresponds to ∼18% of the total K-luminosity (Carballo et al. 1998). Here, we assumed that most of the luminosity is produced within the core radius of the stellar distribution ($\lesssim$1 kpc; see de Ruiter et al. 2005). As the quasar emission dominates over the starlight in the IR and UV bands in the knot reference frame, we neglected the starlight contribution.

In quasars jets, the observed X-ray emission from resolved knots can often be consistently explained via Compton scattering of CMB photons (Tavecchio et al. 2000; Celotti et al. 2001). The energy density of the CMB photons ($U'_{\rm CMB}$) in the jet frame is

$$U'_{\rm CMB} \sim aT^4_{\rm CMB}(1+z)^4\Gamma^2_{\rm (knot/hotspot)}, \quad (3)$$

where $T_{\rm CMB}$ is the temperature of the CMB at $z = 0$. This mechanism is efficient for highly relativistic plasma motion ($\Gamma \gtrsim 10$), but requires also small θ in order to have the observed flux not relativistically de-boosted.

Celotti et al. (2001) have shown that in highly relativistic sources, the CMB radiation becomes the dominant field at $z_d \approx 30$ kpc for $z = 0$. 3C 186 is at high redshift but has a small linear size, it is likely not closely aligned to the observer line of sight, and the assumed bulk motion is "low." Nevertheless, we included the CMB photon field in our analysis for comparison with the case of giant radio sources.

External synchrotron photons. The energy density of the synchrotron radiation from the blazar-like component (see Figure 3) in the reference frame of the knots was estimated as (Celotti et al. 2001)

$$U'_{in} \sim \frac{L^i_{\rm syn,bl.}\Gamma^4_{\rm in}}{4\pi z_d^2 c\Gamma^2_{\rm (knot/hotspot)}}, \quad (4)$$

where $L^i_{\rm syn,bl.}$ is the intrinsic blazar-like synchrotron emission, and the distance between the two radiating regions (i.e., the blazar-like and the knots) is approximated as z_d. The knots and hotspot correspond to the mildly relativistic knot $k_{\rm out}$ in the sketch. We used the observed radio luminosity of the core to normalize $L^i_{\rm syn,bl.}$. Bulk Lorentz factor values between 10 and 20 are usually adopted to model the SED of blazar sources (Celotti & Ghisellini 2008; Ghisellini et al. 2010), with a few extreme cases of blazars in flaring state (for instance, in PKS 2155−304 the SSC modeling requires $\Gamma \approx 100$; Finke et al. 2008). Here, we assumed a moderate bulk motion of the blazar-like component, $\Gamma_{\rm in} = 10$, which gives an intrinsic synchrotron luminosity $L^i_{\rm syn}(k1) = 8.5\times10^{44}$ erg s^{-1}.

Indeed, we do expect that the blazar-like component also emits via IC, and the energy density of the blazar IC photons in the reference frame of the external knot can be calculated in the same way as $U'_{\rm in}$, once we replace $L^i_{\rm syn,bl.}$ with the intrinsic (blazar) IC luminosity. However, these high-energy photons are upscattered to energies higher than the X-ray band we are considering here, and for this reason we do not include them in our analysis.

In Figure 4, we show the energy densities of the above photon fields as a function of the distance z_d for a jet (i.e., a knot in our approximation) with a bulk motion of $\Gamma = 1.4$. The de-projected positions of the two knots (assuming $\theta = 30^\circ$) and the hotspot in the 3C 186 jet are marked by vertical lines and the values of the local synchrotron fields (i.e., seed photons for the SSC) $U'_{\rm SSC}$ are represented by solid points.

The blazar radiation field ($U'_{\rm in}$) is the dominant one even at large scales (≈20 kpc). For comparison, in addition to $\Gamma_{\rm in} = 10$ we also report the case in which the jet has no velocity structure (i.e., $\Gamma_{\rm in} = 1.4$): the nuclear fields, $U'_{\rm disk,torus}$, are the most intense at the scale of the first knot $k2$ ($z_d \lesssim 3$ kpc). Due to the intensity of the disk radiation, $U'_{\rm disk}$ can be higher than, or comparable with, the local synchrotron emission $U'_{\rm SSC}$ up to the hotspot distance ($z_d \approx 15$ kpc). We note that $U'_{\rm CMB}$ is relatively less important below $z_d \approx 20$ kpc, as the amplification factor related to the knot bulk motion is small ($\Gamma^2_{\rm knot} \approx 2$).

4.1.3. Multiwavelength Mapping Results

The comparison of the photon fields shows that the nuclear photons and the "beamed" external synchrotron radiation dominate at the scales of the first knot $k2$. In addition, $U'_{\rm disk}$ and $U'_{\rm in}$ are more intense than, or comparable with, $U'_{\rm SSC}$ even at the hotspot distance. This and the fact that the volumes and energy densities of electrons in the knots and hotspot are similar imply that the bulk of the IC emission should be dominated by the component closer to the nuclear region. Thus, the emission from $k2$ provides a reasonable model approximation to model the jet high-energy emission. In the model of the structured jet, $k2$ corresponds to the slow-moving knot ($k_{\rm out}$ in Figure 3).

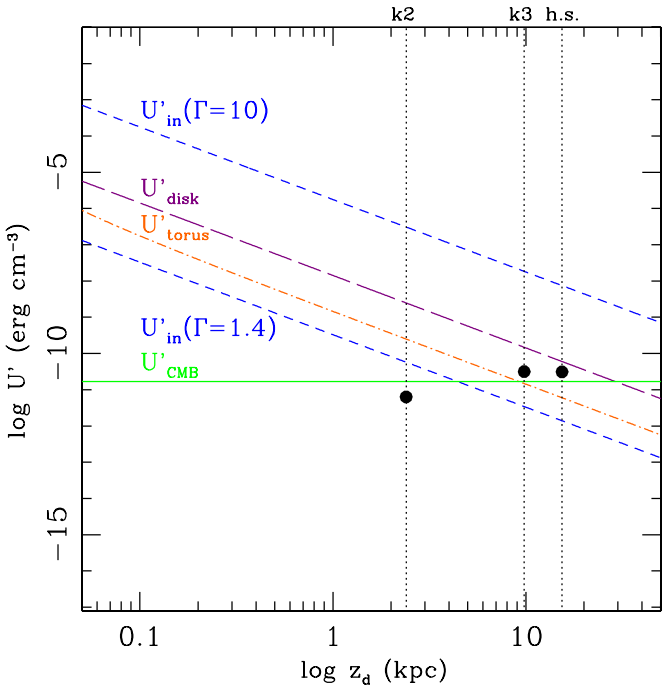

Figure 4. Energy densities as a function of the distance from the base of the jet z_d in the reference frame of the mildly relativistic ($\Gamma = 1.4$) knot (see the sketch in Figure 3). The external photon fields are $U'_{\rm disk}$ (long-dashed), $U'_{\rm torus}$ (dot-dashed), $U'_{\rm CMB}$ (solid), and $U'_{\rm in}$ (short-dashed). The energy density of the external synchrotron photons are estimated for a highly relativistic ($\Gamma = 10$) knot (blazar-like) and, for comparison, for a mildly relativistic knot ($\Gamma_{\rm in} = 1.4$). The dotted vertical lines mark the de-projected position of the two knots and the hotspot in 3C 186 and the black circles correspond to the energy densities of the local synchrotron fields ($U'_{\rm SSC}$). The projected distance scale assumes $\theta = 30^\circ$.

(A color version of this figure is available in the online journal.)

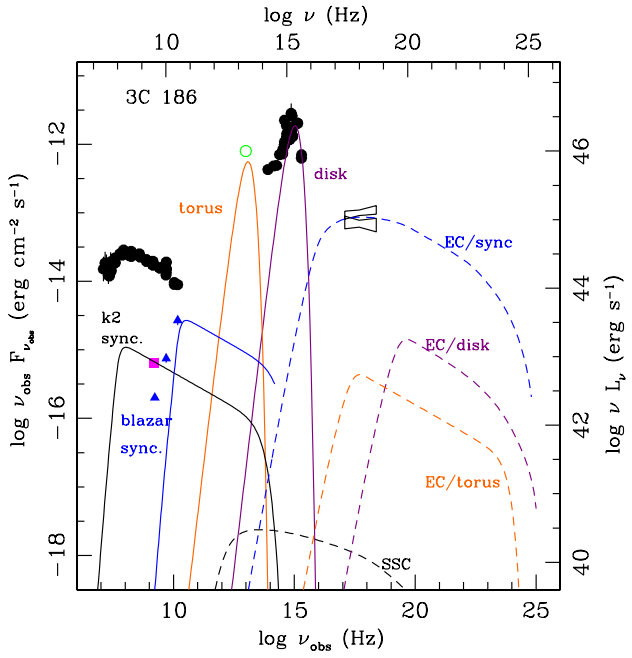

Figure 5. Data and modeled SED of the knot $k2$, located at ∼2.4 kpc distance from the jet apex. Data: black solid circles, green empty circle, and the bow-ties are the radio to X-ray unresolved fluxes from the ASDC archive, *Spitzer* observatory, and *Chandra* 2002 and 2007 observations (see the text), respectively (bow-ties show 90% range). The magenta solid square is the 1.6 GHz flux for $k2$ and the blue solid triangles are the radio fluxes for the core, $k1$ (Spencer et al. 1991). Model: the black solid line (labeled k2 sync.) is the $k2$ synchrotron emission, the orange and violet solid lines are the torus and disk emission (labeled torus and disk, respectively), and the blue solid line (labeled blazar sync.) is the synchrotron emission of the core, blazar-like, component (see the text). The dashed lines correspond to the Comptonization of the synchrotron and nuclear photons with color correspondence with the seed photons as follows: SSC emission indicates the black dashed line, orange and violet dashed lines indicate the upscatterd torus (EC/torus) and disk (EC/disk) fluxes, and the blue dashed line is the EC of the external core synchrotron photons (EC/syn).

(A color version of this figure is available in the online journal.)

In Figure 5, we show the results of the SED modeling of the $k2$ knot emission together with the observed 3C 186 SED. The black points are the multiwavelength data taken from the ASDC archive,[11] the green one is the *Spitzer* flux ($F_{15\,\mu{\rm m}(1+z)} = 8.2 \pm 0.6$ mJy; Leipski et al. 2010) and the bow-ties the 2 keV fluxes from the data of the 2007 (higher value) and 2002 (lower value) *Chandra* observations.[12] The synchrotron emission of $k2$ (black solid line) is normalized to the 1.6 GHz flux (magenta point). Disk (violet solid line) and torus (orange solid line) have been modeled as simple blackbody emission peaking at $\sim 10^{15}$ Hz and $\sim 10^{13}$ Hz, respectively. The synchrotron emission of the blazar-like component is normalized using the observed radio emission of the core ($k1$), assuming a spherical region of radius $R_{\rm in} \sim 0.1$ pc, moving with $\Gamma_{\rm in} = 10$ in a magnetic field $B'_{\rm in} \sim 1$ G. The dashed lines represent the Comptonization of the non-thermal, local (SSC) and the external synchrotron (EC/syn) photons, and of the thermal, disk (EC/disk) and torus (EC/torus) photons by the relativistic electrons in the $k2$ knot.

In the high-energy band (X- to γ-rays), the SSC emission gives a negligible contribution ($L_{\rm SSC} \leqslant 10^{40}$ erg s^{-1}). The luminosities of the EC/disk and EC/torus (in the observer rest frame) can reach a few 10^{43} erg s^{-1}, still below the observed X-ray emission. The EC/torus and EC/disk luminosities peak at different frequencies: the upscattered torus photons are mostly observed in the 2–10 keV band and the bulk of the Comptonized UV photons above 10^{19} Hz. We note that the slope of the EC/disk curve differs (in the high-energy part) from the EC/torus one because in the first case the Compton scattering occurs in the Klein–Nishina regime. Overall, the contribution of the inverse Compton emission off the nuclear (disk/torus) and local synchrotron photon fields is not significant in the X-ray band. We will discuss in Section 5 how this result is affected by our assumptions. We also estimated the IC X-ray luminosity of the blazar-like component in the observer rest frame, considering external Compton on BLR and IR photons (Sikora et al. 1994; Błażejowski et al. 2000; Sikora et al. 2009) and obtained values of $\lesssim 10^{44}$ erg s^{-1}. However, with the same knot parameters, in the framework of the structured-jet model, the observed 2007 *Chandra* flux can be generated via upscattering of the synchrotron photons from the blazar-like component. Note that for compact (GPS) radio sources, the same mechanism could also efficiently produce X-ray emission if the beamed synchrotron photons are IC-scattered by the electrons in the lobes.

5. DISCUSSION

In 3C 186, we aimed at estimating the jet contribution to the total X-ray emission by modeling its broadband SED. The results of the modeling show that the IC X-ray emission of the jet does not provide a relevant contribution except when Compton scattering off the beamed synchrotron emission from a blazar-like knot is considered.

[11] http://tools.asdc.asi.it/SED/

[12] It is evident that our results do not change in any relevant way by considering the 2002 *Chandra* flux.

The radiative X-ray efficiency of a structured jet is related to the presence of a significant velocity gradient between the two regions (as $U'_{\rm in} \propto \Gamma^4_{\rm in}/\Gamma^2_{\rm knot/hotspot}$). Furthermore, this configuration accounts for the properties of relatively misaligned sources: the strongly beamed emission of the blazar component is mostly hidden from the observer view,[13] while the radiation from the slow knot is emitted quasi-isotropically($\delta_{k_{\rm out}/k2} \sim 1.8$ for the mildly relativistic knot). At the optically thin radio frequencies ($\gtrsim 5$ GHz), the beamed core-jet emission still dominates over the quasi-isotropic synchrotron emission from the slower knot (Figure 5). This qualitatively agrees with the picture of a jet-related X-ray emission beamed to a lesser degree than the radio one (Miller et al. 2011).

Before considering the implications in terms of the jet dynamics and energetics in the jet structured model, we need to evaluate the robustness of these results. In the following, we discuss the main assumptions and verify if a different but "reasonable" set of parameter values could lead to significantly different conclusions.

Equipartition assumption. Although equipartition (or minimum energy conditions) between magnetic field and particles is usually assumed in relativistic jets, hotspots, and lobes, there are some indications that jet knots could be far from the minimum-power condition and be particle-dominated (Kataoka & Stawarz 2005). If this were the case for the 3C 186 jet, the equipartition assumption leads to an underestimate of the IC fluxes. Nevertheless, for the one-zone jet, rather severe departures from equipartition are required to account for the observed X-ray flux: these span from ∼4 order of magnitudes for the SSC emission to a minimum of ∼2 order of magnitudes in the case of EC/torus emission.

Beaming factor ($\delta(\Gamma, \theta)$). The viewing angle θ and bulk Lorentz factor Γ are parameters constrained together by the observables. A change of θ may determine a modification of the bulk motion or/and intrinsic luminosity.

In the structured-jet scenario, if we assume a smaller value of θ, say $\theta = 10^\circ$, then the blazar-like component becomes radio overluminous with respect to the observed core flux, unless we assume lower values of $\Gamma_{\rm in}$ or/and $L^i_{\rm syn,bl.}$. This implies that $U'_{\rm in}$ decreases and the final EC/syn along with it (leaving unchanged $\Gamma_{\rm out}$).

In the one-zone model, a change of θ is unimportant when the jet/knot is moving with $\Gamma = 1.4$. At $\theta = 10^\circ$, the luminosity of the knot is maximally amplified for $\Gamma \sim 5$ (and $\delta \sim 6$). However, the same relativistic correction applies to both the synchrotron and the SSC luminosities ($\propto \delta^4$), so that the source parameters have to be coherently modified to agree with the observed radio fluxes: a larger δ must correspond to a decrease of the intrinsic quantities (B, $L^i_{\rm syn}$ and thus $U'_{\rm SSC}$), implying that the SSC flux does not increase and still underpredicts the observed X-ray flux.

In the case of the external Compton process, the nuclear photon fields will be severely de-boosted in the frame of the outer knot moving with $\Gamma = 5$ (as $U'_{\rm disk/torus} \propto 1/\Gamma^2$). The case of the isotropic CMB photon field is different. Since $U'_{\rm CMB} \propto \Gamma^2$, a large bulk motion increases the ratio between the Compton and synchrotron, but still low inclination angles are required. For $\theta = 10^\circ$ and $\delta \sim 5.7$ (the combination of parameters which maximizes the "observed" IC/CMB flux at this angle), it is not possible to account for the observed X-ray flux via IC/CMB without assuming a large ratio for the particle to magnetic field density (≈100). In order to avoid the far-from-equipartition problem (see Harris & Krawczynski 2006 for a review), smaller angles, $\theta \lesssim 6^\circ$, not supported by the radio data, and the values of Γ in the range between 10 and 30, are required.

Location of the emitting knot. We identified the sites of the jet X-ray emission with the compact radio features, knots, and a hotspot. In blazars and quasars, the location of the region where the bulk of the jet energy dissipation takes place is a matter of debate. In blazars, γ-ray fast variability provides us with upper limits on the distance from the central black hole of about 0.1–0.3 pc, i.e., still inside the broad-line region. However, this scenario is questioned. Sikora et al. (2009) proposed that the high-energy spectrum could be due to Compton scattering off thermal IR photons by electrons located at parsec scale distances from the nucleus. This would also explain the lack of bulk-Compton and Klein–Nishina features in the blazar spectra.

In 3C 186, moving the dissipative knot to a smaller distance z_d clearly determines an increase of the intensity of the $U'_{\rm disk,torus}$ (see Figure 4). For a mildly relativistic knot ($\Gamma = 1.4$), the EC/torus emission can, in principle, reach the observed X-ray flux at $z_d \sim 100$ pc. However, this estimate does not account for the decrease of the region volume consequent to the smaller jet cross-section. Higher EC/torus luminosities can be obtained if the knot is moving within the torus regions, as proposed for the X-ray emission of the quasar PKS 1127–145 (Błażejowski et al. 2004). Nevertheless, this also require a small θ and large Γ (in PKS 1127–145 $\Gamma = 10$ and $\theta \sim 5^\circ$; Błażejowski et al. 2004), not supported by the 3C 186 data.

5.1. Implications of a Structured Jet

The above discussion on the main parameters confirms that it is hard to accommodate the observed 3C 186 X-ray emission with a jet origin in the framework of a single-zone scenario. At the same time, the model which can successfully reproduce the observed X-ray emission in terms of jet emission implies a structured jet. This has important consequences, not only for the jet radiative efficiency, but also for its dynamics and energetics.

Jet dynamics. A significant reduction in the velocity of the jet with an increasing distance from the center is the determining factor to ensure its radiative efficiency in the adopted scenario. In giant radio sources, the hotspots likely have sub-relativistic velocities, however the jet/knot dynamics are still uncertain. In FRII sources, the detection of X-ray emission from knots is commonly explained with the IC/CMB mechanism (Tavecchio et al. 2000; Celotti et al. 2001) and implies relativistic jet velocities ($\Gamma \approx 10$) on kiloparsec scales.

On the other hand, radio observations support a significant deceleration from parsec to kiloparsec scales, with characteristic jet speeds at kiloparsec distances in the range between $0.6c$ and $0.7c$ (Wardle & Aaron 1997). Mullin & Hardcastle (2009) adopted a Bayesian parameter-inference method to constrain the jet Lorentz factors for a complete sample of FRII with $z < 1$ and found bulk motions of $\Gamma \approx 10$–14 and $\Gamma \approx 1.18$–1.49 in the beams on parsec and kiloparsec scales, respectively. While the parsec-jet velocities agree with the ones inferred from very long baseline interferometry observations (Lister et al. 2009 and references therein), the results on the kiloparsec jet challenge the beamed IC/CMB models. Jet deceleration is also proposed to reconcile the discrepancy between the estimated jet speeds at

[13] The observed (monochromatic) synchrotron/SSC luminosity goes as $\delta^{3+\alpha}_{\rm bl.}$, where the Doppler factor is defined as $\delta = [\Gamma(1 - \beta\cos\theta)]^{-1}$ and $\beta = v/c$, while the external Compton radiation follows the pattern $\propto \delta^{4+2\alpha}_{\rm bl.}$ (Dermer 1995) and, for the assumed values of θ and $\Gamma_{\rm in}$ in 3C 186, $\delta_{\rm bl.} \sim 0.7$.

kiloparsec scales and the bulk motions required by the IC/CMB model (see Hardcastle 2006 for the case of lobe-dominated quasars and FRII radio galaxies, and Marshall et al. 2011 for the study of a subsample of flat spectrum radio quasars observed by *Chandra*).

The mechanism which would be responsible for the jet deceleration is still not clear. Entrainment of external interstellar medium seems to be less important in powerful FRIIs and quasars, which display well-collimated jets on hundreds of kiloparsec scales. Interactions with the surrounding medium are instead satisfactorily invoked to explain the presence of a multi-layer structure in the jets of FRI sources (see the case of 3C 31; Laing & Bridle 2002a, 2002b).

In the spine-layer model (e.g., Ghisellini et al. 2005), the two regions are cospatial. Thus, the radiative feedback takes place at the same jet scales (z_d), different from our case where the interactive regions are located at kiloparsec distance. In the latter case, the observations can partly resolve, and thus provide us with constraints on both the regions (Georganopoulos & Kazanas 2003). In the spine-layer scenario, the radio emission might be completely dominated by one of the two components, preventing us to constrain the model parameters of the other.

Finally, we note that a critical issue for the structured-jet model is represented by the one-sidedness of the radio source. The detection of only one jet at radio frequencies is usually explained in terms of beamed radiation and suggests that the jets are moving with relativistic speeds. The crucial assumption here is that the radio source is symmetric and the same physical conditions occur in the jet and counterjet. Nevertheless, several studies have shown that mildly relativistic speeds are sufficient to account for the observed jet sidedness ($\beta \approx 0.4$–0.7; Wardle & Aaron 1997; Hardcastle et al. 1999; Arshakian & Longair 2004; Mullin & Hardcastle 2009). Given the assumed θ, our adopted bulk motion is consistent with the minimum value ($\Gamma \gtrsim 1.25$) necessary to reproduce the observed jet/counterjet ratio lower limit,[14] $J \gtrsim 81$ (measured from the MERLIN 5 GHz map at $\sim 0\farcs05$ resolution presented in Ludke et al. 1998; C.C. Cheung 2012, private communication).

We now consider the observed 3C 186 X-ray variability in the framework of the structured jet. Blazars are typically variable at radio wavelengths (with different intensities and timescales). If the Unified Model (Urry & Padovani 1995) is correct and the base of the jet of 3C 186 hosts a blazar region, then its putative radio variability also implies a change in $U'_{\rm in}$ and thus in the observed EC/syn flux. The X-ray variability can be accounted for by a corresponding variation (about a factor of 1.4) of the observed core radio flux (e.g., the radio flux of $k1$) that could be caused either by a fluctuation of the intrinsic luminosity $L'_{\rm syn,bl.}$ or by an increase of the bulk motion $\Gamma_{\rm in}$. However, the propagation time of the blazar synchrotron photons to $k2$ introduces a significant delay ($\approx$8000 yr) between the radio and X-ray flux variation and makes this hypothesis difficult to be tested. If the X-ray flux variation is instead due to a change in the distribution of the emitting electrons in $k2$, then high-resolution radio observations should be able to detect a simultaneous variation of the radio and X-ray flux.

Jet power. An estimate of the total power carried by the jet can be inferred from the physical parameters adopted to model the two emitting regions of the structured jet. The kinetic powers in particles and the magnetic field were estimated as follows:

$$L_i = \pi R^2 \Gamma^2 \beta c U'_i, \quad (5)$$

where U'_i is the energy density, in the comoving frame, of electrons, $U'_e = m_e c^2 n_e \langle\gamma\rangle$, cold protons, $U_p = m_p c^2 n_p$, and the magnetic field, $U'_B = B^2/8\pi$. Here, we assumed one cold proton per electron ($n_p = n_e$), m_e and m_p are the electron and proton masses, respectively, and $\langle\gamma\rangle$ is the average electron Lorentz factor.

The analogous component associated to radiation, i.e., the radiatively dissipated power, is

$$L_r = \pi R^2 \Gamma^2 c U'_{\rm rad} \approx L' \Gamma^2, \quad (6)$$

where L' is the intrinsic total rest-frame (synchrotron and IC) luminosity.

Table 4
3C 186 Jet Powers for the Structured-jet Model (see Figure 3)

Luminosities (erg s^{-1})	Blazar-like Component/ Core	$k_{\rm out}/k2$
L_e	3.2×10^{46}	3.7×10^{45}
L_p	1.1×10^{48}	5.2×10^{46}
L_B	2.1×10^{47}	9.4×10^{44}
$L_{\rm kin}$	1.13×10^{48}	5.6×10^{46}
L_r	1.1×10^{47}	1.0×10^{45}

Notes. Powers associated with the bulk motion of (emitting) relativistic electrons (L_e), cold protons (L_p), and pointing flux (L_B). $L_{\rm kin}$ is the total jet kinetic power and L_r is the radiatively emitted power.

The energetics of the two emitting regions in the 3C 186 jet are shown in Table 4. The values obtained for $k2$ are rather standard for powerful sources, while the kinetic power corresponding to the blazar-component parameters ($L_{\rm kin} = 1.4 \times 10^{48}$ erg s^{-1}) is at the high-energy tail with respect to what is usually found in blazar sources (ranging between 10^{46} and 10^{48} erg s^{-1}; Celotti & Ghisellini 2008; Ghisellini et al. 2009, 2010). Indeed, the assumption on the jet composition affects the value of $L_{\rm kin}$ in a critical way. In the "opposite" case of a purely electron–positron plasma, the jet would be magnetically dominated ($L_B = 2.1 \times 10^{47}$ erg s^{-1}) and highly dissipative ($L_r = 1.1 \times 10^{47}$ erg s^{-1}).

The debate on the jet composition is still open. Based on X-ray observations, Sikora & Madejski (2000) argued in favor of a jet containing more e^+e^- pairs than protons, but dynamically still dominated by protons. Similar conclusions have been reached by Stawarz et al. (2007), for the case of the hotspots and jet of Cygnus A, and by Celotti & Ghisellini (2008). Similarly, Ghisellini & Tavecchio (2010) placed an upper limit of 10 pairs per proton ($n_e \lesssim 10 n_p$) in the relativistic jets of FSRQs, in order to prevent radiation drag (Odell 1981; Sikora et al. 1996; Ghisellini et al. 2005, and references therein) when the dominant radiative process is external Compton.

The radiative power is a less model-dependent quantity, relying only on the assumption on the bulk motion and θ, and provides us with lower limits of the jet power of $\approx 10^{47}$ erg s^{-1} and $\approx 10^{45}$ erg s^{-1} for the blazar-like component and the mildly relativistic knot, respectively.

Siemiginowska et al. (2010) estimated the jet power from the relation between the radio luminosity at 151 MHz and the jet power itself (Willott et al. 1999) finding $L_{\rm kin} = 2.4 \times 10^{45}$ erg s^{-1}. Considering the scatter in the relation and the

[14] Here, we estimated the jet speed $\beta \gtrsim 0.55$ ($\Gamma \gtrsim 1.25$) from Equation (A10) in Urry & Padovani (1995) for $\theta = 30^\circ$ in the case of a moving isotropic source. Assuming a continuous jet, we obtain a slightly larger—but still consistent with our value—limit, $\beta \gtrsim 0.7$ ($\Gamma \gtrsim 1.4$).

uncertainties on the composition, this is not too far from the $L_{\rm kin}$ calculated for the mildly relativistic knot $k2$ (and consistent with the $L_{\rm kin}$ lower limit provided by the radiative power).

The difference in $L_{\rm kin}$ between the blazar component and the knot, about two orders of magnitude, points to a jet which (radiatively) dissipates much more efficiently, $\sim$10% of the total power, on the blazar scales. Nevertheless, if the above estimates are reliable, it remains unclear in which form the rest of kinetic energy is released. Alternatively, we might be underestimating the knot kinetic power as this refers to the radiating component only. A further possibility is that we might be observing two subsequent outbursts of different intensity (Reynolds & Begelman 1997; Czerny et al. 2009). Support for the idea of intermittent activity in radio sources comes from the observations of radio relics and radio sources with a double–double morphology (i.e., with two aligned but unequally sized pairs of lobes; Lara et al. 1999; Schoenmakers et al. 2000; Saikia et al. 2006; Jamrozy et al. 2007).

The jet power of the blazar-like component is larger than, or at least comparable with, the accretion disk luminosity ($L'_{\rm disk} \sim 10^{47}$ erg s^{-1}; Siemiginowska et al. 2010). Recent studies of blazars, based on high-energy (X- to γ-ray) observations, find that the jet power is proportional to (but larger than) the disk luminosity (Ghisellini et al. 2010). If this is the case for 3C 186, then the radiative feedback between the source and its environment might be energetically driven by the jet rather than by the accretion power, depending on the modality in which the power is conveyed into the ambient medium.

6. SUMMARY

We investigated the contribution of the jet emission to the total high-energy radiation observed in the compact, young, and powerful quasar 3C 186. The results of the spectral analysis, based on a deep *Chandra* observation, are ambiguous. The best-fit model, a single power law with a steep slope ($\Gamma = 1.92 \pm 0.03$ and a 2–10 keV luminosity $L_{2-10} = (1.15 \pm 0.04) \times 10^{45}$ erg s^{-1}), is compatible with non-thermal emission from the extended radio jets and lobes as well as thermal emission related to the central accretion.

In order to place quantitative constraints on the jet X-ray contribution, we modeled its broadband emission with a leptonic synchrotron-IC model. The most relevant photon fields at the jet scales have been taken into account as possible IC target photons.

The SED modeling shows that in the framework of a single-zone model, the jet emission is not relevant in the X-ray band (for the set of main physical parameter values favored by the observables).

Different results are obtained when the hypothesis of a single emitting zone is relaxed. We considered a jet with a velocity structure, exemplified by two emitting regions with different velocities, namely a blazar-like component and an external, mildly relativistic knot.

We find that an X-ray flux comparable with the *Chandra* observed one can be produced via Compton scattering off beamed synchrotron emission from a blazar-like emitting region by the relativistic electrons in a knot located at kiloparsec scales. Hence, in 3C 186 the relevance of the jet as a source of high-energy radiation seems intimately related to its dynamical structure. Indeed, this does not rule out the possibility of a competing contribution of the disk–corona to the X-ray emission. We note that the estimates of the X-ray emission related to the accretion disk based on Koratkar & Blaes (1999) give $L_X \sim L_{\rm UV}/10^{1.5} \sim 2 \times 10^{45}$ erg s^{-1}, similar to the observed X-ray luminosity. The detection of 3C 186 at γ-ray energies would be decisive to discriminate the nature of its X-ray emission. Unfortunately, the predicted flux of the model is more than two orders of magnitude below the detection limit of the *Fermi*-LAT (Atwood et al. 2009). In the framework of the structured jet, radio variability correlated to the observed X-ray one can be detected if it is caused by a change in the electron population of the mildly relativistic knot, but not if it is related to a variation of the blazar component.

There are some interesting aspects related to the structured-jet scenario considered here. Dynamically, the jet has to decelerate on kiloparsec scales. It requires an initial high jet kinetic power ($L_{\rm kin} \sim 10^{48}$ erg s^{-1}) that is comparable with those estimated for the most powerful blazars. Unless time dependent, in which case one should expect to find sources where the kiloparsec scale power exceeds that associated with the blazar component, the jet has to experience strong dissipation on kiloparsec scales to account for the difference in the jet power estimated using the physical parameters of the two emitting regions. Depending on the assumptions on the composition, the initial jet power could be up to two orders of magnitude larger than the disk luminosity. Therefore, in such a case, the interactions, with the host-galaxy medium first and the cluster environment then, could be dominated by the jet.

The study of 3C 186 is a pilot case for a broader investigation of radiation processes in young radio sources. In our future work we will extend the modeling presented here to other young radio sources observed in X-rays, in order to (1) determine whether there is a consistent behavior with respect to the possible jet contribution and (2) ascertain whether there are candidates suitable for detection in the γ-ray band to definitely assess the origin of the high-energy emission in the early phases of the radio sources' growth.

We thank the anonymous referee for comments that significantly improved the manuscript. The authors thank C.C. Cheung for providing radio fluxes, M.Guainazzi, Ł.Stawarz for useful discussions, and T. Aldcroft for help in improving the text. G.M. thanks P.Grandi, M.Sobolewska, and F.Massaro for valuable discussions and suggestions. G.M. is grateful to L.Ostorero for insightful comments and great help in improving the manuscript. This research is funded in part by NASA contract NAS8-39073. Partial support for this work was provided by *Fermi* grant NNX10AO60G. Partial support for this work was provided by the National Aeronautics and Space Administration through Chandra Award Number GO2-3148A and GO8-9125A, GO0-11133X issued by the Chandra X-Ray Observatory Center, which is operated by the Smithsonian Astrophysical Observatory for and on behalf of NASA under contract NAS8-39073. A.C. thanks the Center for Astrophysics for hospitality.

REFERENCES

Arshakian, T. G., & Longair, M. S. 2004, MNRAS, 351, 727
Atwood, W. B., Abdo, A. A., Ackermann, M., et al. 2009, ApJ, 697, 1071
Avni, Y., & Tananbaum, H. 1982, ApJ, 262, L17
Begelman, M. C. 1999, in The Most Distant Radio Galaxies, ed. H. J. A. Rottgering, P. N. Best, & M. D. Lehnert (Amsterdam: Royal Netherlands Acad. Arts and Sciences), 173
Belsole, E., Worrall, D. M., & Hardcastle, M. J. 2006, MNRAS, 366, 339
Błażejowski, M., Siemiginowska, A., Sikora, M., Moderski, R., & Bechtold, J. 2004, ApJ, 600, 27
Błażejowski, M., Sikora, M., Moderski, R., & Madejski, G. M. 2000, ApJ, 545, 107

Bloom, S. D., & Marscher, A. P. 1996, ApJ, 461, 657
Bridle, A. H., & Perley, R. A. 1984, ARA&A, 22, 319
Carballo, R., Sanchez, S. F., Gonzales-Serrano, J. I., Benn, C. R., & Vigotti, M. 1998, AJ, 115, 1234
Celotti, A., & Ghisellini, G. 2008, MNRAS, 385, 283
Celotti, A., Ghisellini, G., & Chiaberge, M. 2001, MNRAS, 321, 1
Chatterjee, R., Marscher, A. P., Jorstad, S. G., et al. 2011, ApJ, 734, 43
Chiaberge, M., Capetti, A., & Celotti, A. 1999, A&A, 349, 77
Chiaberge, M., Celotti, A., Capetti, A., & Ghisellini, G. 2000, A&A, 358, 104
Czerny, B., Siemiginowska, A., Janiuk, A., Nikiel-Wroczyński, B., & Stawarz, Ł. 2009, ApJ, 698, 840
Dermer, C. D. 1995, ApJ, 446, L63
Dermer, C. D., & Schlickeiser, R. 1993, ApJ, 416, 458
de Ruiter, H. R., Parma, P., Capetti, A., et al. 2005, A&A, 439, 487
Evans, I. N., & Koratkar, A. P. 2004, ApJS, 150, 73
Fan, J. H., & Zhang, J. S. 2003, A&A, 407, 899
Fanti, R., Fanti, C., Schilizzi, R. T., et al. 1990, A&A, 231, 333
Finke, J. D., Dermer, C. D., & Bottcher, M. 2008, ApJ, 686, 181
Freeman, P., Doe, S., & Siemiginowska, A. 2001, Proc. SPIE, 4477, 76
Georganopoulos, M., & Kazanas, D. 2003, ApJ, 589, L5
Ghisellini, G., & Madau, P. 1996, MNRAS, 280, 67
Ghisellini, G., & Tavecchio, F. 2010, MNRAS, 409, L79
Ghisellini, G., Tavecchio, F., Bodo, G., & Celotti, A. 2009, MNRAS, 393, L16
Ghisellini, G., Tavecchio, F., & Chiaberge, M. 2005, A&A, 432, 401
Ghisellini, G., Tavecchio, F., Foschini, L., et al. 2010, MNRAS, 402, 497
Ghisellini, G., Tavecchio, F., & Ghirlanda, G. 2009, MNRAS, 399, 2041
Giovannini, G., Cotton, W. D., Feretti, L., Lara, L., & Venturi, T. 1999, Mem. Soc. Astron. Ital., 70, 161
Giroletti, M., Giovannini, G., Feretti, L., et al. 2004, ApJ, 600, 127
Grandi, P., & Palumbo, G. G. C. 2004, Science, 306, 998
Grandi, P., & Palumbo, G. G. C. 2007, ApJ, 659, 235
Guainazzi, M., Siemiginowska, A., Stanghellini, C., et al. 2006, A&A, 446, 87
Gugliucci, N. E., Taylor, G. B., Peck, A. B., & Giroletti, M. 2005, ApJ, 622, 136
Haas, M., Willner, S. P., Heymann, F., et al. 2008, ApJ, 688, 122
Hardcastle, M. J. 2006, MNRAS, 366, 1465
Hardcastle, M. J., Alexander, P., Pooley, G. G., & Riley, J. M. 1999, MNRAS, 304, 135
Hardcastle, M. J., & Worrall, D. A. 2000, MNRAS, 314, 969
Harris, D. E., & Krawczynski, H. 2006, ARA&A, 44, 463
Jamrozy, M., Konar, C., Saikia, D. J., et al. 2007, MNRAS, 378, 581
Jester, S., Harris, D. E., Marshall, H. L., & Meisenheimer, K. 2006, ApJ, 648, 900
Kataoka, J., Reeves, J. N., Iwasawa, K., et al. 2007, PASJ, 59, 279
Kataoka, J., & Stawarz, Ł. 2005, ApJ, 622, 797
Kellermann, K. I., Sramek, R., Schmidt, M., Shaffer, D. B., & Green, R. 1989, AJ, 98, 1195
Kelly, B. C., Bechtold, J., Siemiginowska, A., Aldcroft, T., & Sobolewska, M. 2007, ApJ, 657, 116
Koratkar, A., & Blaes, O. 1999, PASP, 111, 1
Kuraszkiewicz, J. K., Green, P. J., Forster, K., et al. 2002, ApJS, 143, 257
Laing, R. A., & Bridle, A. H. 2002a, MNRAS, 336, 328
Laing, R. A., & Bridle, A. H. 2002b, MNRAS, 336, 1161
Lara, L., Márquez, I., Cotton, W. D., et al. 1999, A&A, 348, 699
Leipski, C., Haas, M., Willner, S. P., et al. 2010, ApJ, 717, 766
Lister, M. L., Cohen, M. H., Homan, D. C., Kadler, M., & Kellerman, K. I. 2009, AJ, 138, 1874
Ludke, E., Garrington, S. T., Spencer, R. E., et al. 1998, MNRAS, 299, 467
Lyutikov, M., & Lister, M. 2010, ApJ, 722, 197
Maraschi, L., Ghisellini, G., & Celotti, A. 1992, ApJ, 397, L5
Marscher, A. P., Jorstad, S. G., Larionov, V. M., et al. 2010, ApJ, 710, L126
Marshall, H. L., Gelbord, J. M., Schwartz, D. A., et al. 2011, ApJS, 193, 15
McConville, W., Ostorero, L., Moderski, R., et al. 2011, ApJ, 738, 148
Miller, B. P., Brandt, W. P., Schneider, D. P., et al. 2011, ApJ, 720, 20
Mullin, L. M., & Hardcastle, M. J. 2009, MNRAS, 398, 1989
Murgia, M., Fanti, C., Fanti, R., et al. 1999, A&A, 345, 769
Nan, R., Schilizzi, R. T., Fanti, C., & Fanti, R. 1991, A&A, 252, 513
Nelder, J. A., & Mead, R. 1965, Comput. J., 7, 308
Netzer, H., Heller, A., Loinger, F., et al. 1996, MNRAS, 279, 429
O'Dea, C. P. 1998, PASP, 110, 493
Odell, S. L. 1981, ApJ, 243, 147
Ostorero, L., Moderski, R., Stawarz, Ł., et al. 2010, ApJ, 715, 107
Owsianik, I., Conway, J. E., & Polatidis, A. G. 1998, A&A, 336, L37
Poutanen, J., & Stern, B. 2010, ApJ, 717, L118
Reynolds, C. S., & Begelman, M. C. 1997, ApJ, 487, L135
Saikia, D. J., Konar, C., & Kulkarni, V. K. 2006, MNRAS, 366, 1391
Sambruna, R. M., Gambill, J. K., Maraschi, L., et al. 2004, ApJ, 608, 698
Sambruna, R. M., Reeves, J. N., Braito, V., et al. 2009, ApJ, 700, 1473
Scheuer, P. A. G., & Readhead, A. C. S. 1979, Nature, 277, 182
Schoenmakers, A. P., de Bruyn, A. G., Rottgering, H. J. A., van der Laan, H., & Kaiser, C.R. 2000, MNRAS, 315, 371
Siemiginowska, A. 2009, Astron. Nachr., 330, 264
Siemiginowska, A., Bechtold, J., Aldcroft, T. L., et al. 2002, ApJ, 570, 543
Siemiginowska, A., Burke, D. J., Aldcroft, T. L., et al. 2010, ApJ, 722, 102
Siemiginowska, A., Cheung, C. C., LaMassa, S., et al. 2005, ApJ, 632, 110
Siemiginowska, A., LaMassa, S., Aldcroft, T. L., Bechtold, J., & Elvis, M. 2008, ApJ, 684, 811
Siemiginowska, A., Stawarz, Ł., Cheung, C. C., et al. 2007, ApJ, 657, 145
Sikora, M., Begelman, M. C., & Rees, M. J. 1994, ApJ, 421, 153
Sikora, M., & Madejski, G. 2000, ApJ, 534, 109
Sikora, M., Sol, H., Begelman, M. C., & Madejski, G. M. 1996, MNRAS, 280, 781
Sikora, M., Stawarz, L., Moderski, R., Nalewajko, K., & Madejski, G. 2009, ApJ, 704, 38
Simpson, C., & Rawlings, S. 2000, MNRAS, 317, 1023
Sobolewska, M., Gierlinski, M., & Siemiginowska, A. 2009, MNRAS, 394, 160
Spencer, R. E., Schilizzi, R. T., Fanti, C., et al. 1991, MNRAS, 250, 225
Stawarz, Ł., Cheung, C. C., Harris, D. E., & Ostrowski, M. 2007, ApJ, 662, 213
Stawarz, Ł., Ostorero, L., Begelman, M. C., et al. 2008, ApJ, 680, 911
Stawarz, Ł., & Ostrowski, M. 2002, ApJ, 578, 763
Sutherland, R. S., & Bicknell, G. V. 2007, Ap&SS, 311, 293
Swain, M. R., Bridle, A. H., & Baum, S. A. 1998, ApJ, 507, 29
Tavecchio, F., Maraschi, L., Sambruna, R. M., & Urry, C. M. 2000, ApJ, 544, L23
Tengstrand, O., Guainazzi, M., Siemiginowska, A., et al. 2009, A&A, 501, 89
Urry, C. M., & Padovani, P. 1995, PASP, 107, 803
Vink, J., Snellen, I., Mack, K.-H., & Schilizzi, R. 2006, MNRAS, 367, 928
Wardle, J. F. C., & Aaron, S. E. 1997, MNRAS, 286, 425
Weisskopf, M. C., Brinkman, B., Canizares, C., et al. 2002, PASP, 114, 1
Willott, C. J., Rawling, S., Blundell, K. M., & Lacy, M. 1999, MNRAS, 309, 1017
Worrall, D. M., Birkinshaw, M., Kraft, R. P., et al. 2008, ApJ, 673, L135
Worrall, D. M., Hardcastle, M. J., Pearson, T. J., & Readhead, A. C. S. 2004, MNRAS, 347, 632
Worrall, D. M., Tananbaum, H., Giommi, P., & Zamorani, G. 1987, ApJ, 313, 596
Zamorani, G., Henry, J. P., Maccacaro, T., et al. 1981, ApJ, 245, 357
Zensus, J. A. 1997, ARA&A, 35, 607